JOURNAL OF MATERIALS SCIENCE 1 (1966) 280–295

Defects in Epitaxial Films of Semiconducting Compounds with the Sphalerite Structure

D. B. HOLT
Metallurgy Department, Imperial College, London, SW7, UK

Received 20 May 1966

The crystallography of point defects, dislocations, grain boundaries, misfit dislocation networks, and polytypes in semiconducting compounds with the sphalerite (zincblende) structure is outlined. The methods available for depositing films of compounds are reviewed with reference to the problem of non-stoichiometry. The variation of film structure with substrate temperature is considered, and the few published results of studies of the phase structures and the defect content of epitaxial films of semiconducting compounds are described. The experimental methods available for more detailed analysis of these features are then pointed out.

1. Introduction

Epitaxy has become the subject of a great deal of research [1], largely owing to the pressing need for thin films of controlled and reproducible properties in microminiaturised circuits. Practical interest has chiefly been concerned with films of metals for resistors, dielectrics for capacitors, and silicon for active devices. Interest in thin films of semiconducting compounds has been less intense, and leading applications, such as electroluminescent ZnS panels and thin film, insulated-gate, field-effect CdS transistors, have involved films of ill-defined structure deposited on amorphous substrates. Nevertheless, a result of the slowly growing scientific and technological interest is an increasing literature on epitaxial films of semiconducting compounds.

In this article, attention will be confined to those compounds crystallising in the sphalerite (zincblende) structure. Epitaxial films of a large number of compounds with the sphalerite structure can be produced, and progress is beginning to be made in the study of the defect structures of these films by the application of a number of techniques, but especially by the application of transmission electron microscopy.

2. Crystallography of Defects in Epitaxial Films of Sphalerite-Structure Compounds

Structural defects in epitaxial films of sphalerite-structure compounds must be expected to be much like those in the fcc metals, which have the same space lattice as sphalerite, and especially like those in films of the crystallographically similar diamond-structure elements, Ge and Si. However, two factors imply greater complexity in the defect structure in sphalerite-structure materials. The first is that the sphalerite structure is non-centrosymmetric, so that, for example, the [1 1 1] direction is not equivalent to the $[\bar{1}\,\bar{1}\,\bar{1}]$ direction. The second is that a number of the compounds, especially the II-VI compounds, are polymorphic, i.e. they occur in the $a\alpha$-$b\beta$-$c\gamma$-$a\alpha$-$b\beta$-$c\gamma$ . . . stacking sequence of double {1 1 1} atom planes, the cubic sphalerite structure, and in the $a\alpha$-$c\gamma$-$a\alpha$-$c\gamma$ . . . sequence, the hexagonal wurtzite structure, as shown in fig. 1. In addition, a variety of complicated longer repeat sequences called *polytypes* occur. Polytypic stacking sequences are best represented in projection on a $(1\,1\,\bar{2}\,0)$ plane (indexing the structures as if they were all hexagonal). (For an extended account of polytypism, see reference 2.) A (Ramsdell) stacking diagram in

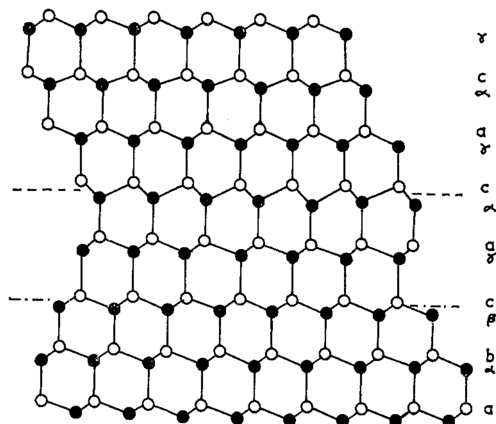

Figure 1 Sphalerite-wurtzite interface. In the lower part of the figure, the double {111} planes are stacked in cyclic permutation of all three of the possible positions aα and bβ and cγ to constitute the cubic sphalerite structure. In the upper part of the diagram, the double atom planes are stacked in cyclic permutation of only two of the positions (aα and cγ in this drawing) to constitute the hexagonal wurtzite structure.

this projection may be made by plotting the stacking positions, a, b, c . . . (omitting the Greek letter planes for brevity), along the abcissa and representing the successive, vertically-stacked double atom planes along the ordinate. The sphalerite structure is represented by a straight line of unit slope, and the wurtzite structure by a vertical single-step zig-zag, as shown in fig. 2. All polytypes can be represented in such a diagram. For example, polytype 6H is a vertical three-step zig-zag, and 15R a three-step-two-step zig-zag.

Nine polytypes have been reported in ZnS

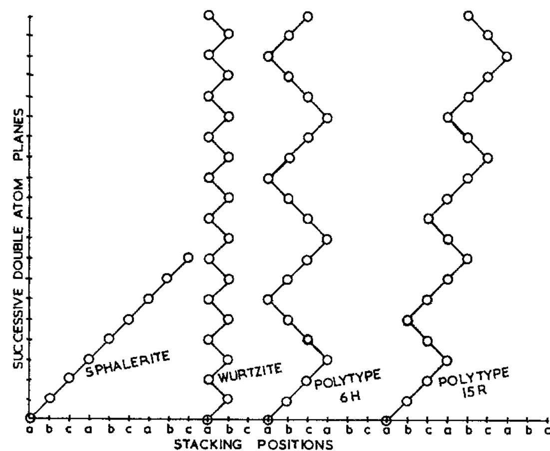

Figure 2 Stacking sequence diagram for representing polytypes.

[3, 4]. In SiC, which has been more intensively studied, 37 polytypes had been identified by 1963 [2]. A 15R polytype has been reported as occurring in ZnTe, and a 12H in CdTe [5]. There is some evidence to indicate that polytypes also occur in the case of CdS and CdSe [5, 6].

In addition, it has been claimed that ZnS transforms from cubic to hexagonal via a transitional rhombohedral polymorph over a range of some hundreds of degrees [7]. Electron microscope observations provide evidence for regions in which many closely spaced faults in the stacking sequence occur in ZnS. In some cases, these fault series corresponded to a direct martensitic transformation from the hexagonal to the cubic structure [8], and, in other cases, the faulting corresponded to regions of twinned cubic material in hexagonal crystals [9]. Thus, stacking sequences corresponding to twins, second phases, polytypes, and stacking disorder [10] may occur in epitaxial films of, at any rate, the II-VI compounds, and must be expected in films of ZnS and SiC.

The effects of the absence of a centre of symmetry in the sphalerite structure on the geometry of the defects may be considered systematically by grouping the defects according to the number of dimensions involved.

2.1. Point Defects and Non-stoichiometry

The number of possible point defect types is twice that in Ge and Si. Thus, both cation and anion vacancies may occur, and both cations and anions may occupy interstitial positions. Geometrical models based on covalent-bonding ideas have been used, together with central force expressions for nearest neighbour interactions, to calculate the formation and migration energies of vacancies in the diamond-structure elements [11-13], but this approach has not yet been extended to the sphalerite-structure compounds. A basically ionic treatment (a modified Mott-Littleton method) has been given for the calculation of the formation energies of Frenkel and of Schottky defects in ZnS. The nearest neighbour interactions were, however, represented by a method which takes some account of the partially covalent nature of the bonding [14].

Values of the energies of the point defects are needed for any quantitative treatment of the important problem of non-stoichiometry in semiconducting compounds. This problem has been discussed in terms of the method of the

grand partition function [15, 16] and also by the minimisation of the molar Gibbs free energy [17]. No experimental investigations of non-stoichiometry in thin films are known to the writer, but several techniques have been applied to the study of non-stoichiometric bulk GaAs crystals. Straumanis and Kim [18] found, by X-ray measurement of lattice parameter, that the intermetallic, sphalerite-structure phase in the GaAs system extends at least from 49.998 to 50.009 at. % As. The sensitivity of their technique was such that the phase could be as much as 0.009 at. % wider than the limits just quoted. While this is a very narrow phase field by ordinary metallurgical standards, the limits correspond to concentrations of about 4×10^{18} As vacancies/cm^3, and about 2×10^{19} Ga vacancies/cm^3, respectively (assuming that non-stoichiometry results in vacancies only). Internal friction measurements on GaAs have been interpreted as indicating the presence of at least 8×10^{18} defects/cm^3 with $<110>$ orthorhombic symmetry. The simplest of the defects, whose occurrence in GaAs is probable, and that fits the internal friction observations, is a Ga di-vacancy on nearest neighbour Ga sites [19]. Electron paramagnetic resonance studies provide evidence for the existence of from 2 to 5×10^{19} lattice defects/cm^3 in vacuum-annealed GaAs containing less than 2×10^{17} impurity atoms/cm^3 [20]. These defects may be multi-atom complexes [24]. Measurements of electrical and thermal properties of GaAs, which has been annealed, or into which impurities have been diffused, provide indirect evidence for the occurrence of large numbers (more than 10^{19}/cm^3 according to reference 24) of point defects [21-24]. The order of magnitude agreement between the point defect concentrations deduced from all these methods of measurement is noteworthy. However, its significance is not clear as the different techniques are sensitive to different types of point defects, i.e. to different members of the series: single vacancies or interstitials; di-vacancies or interstitial atom pairs; and larger point defect clusters.

It has also been reported that the dislocation density in GaAs grown in a horizontal boat depends on the As pressure over the melt, and it was suggested that this was due to the aggregation of vacancies to form dislocation loops [25]. Both Ga and As vacancies may be expected to be electrically active, i.e. to act as donors or acceptors, and to act as recombination or trapping centres. The phase limits of GaAs therefore correspond to degrees of non-stoichiometry equivalent to what are very high doping levels by semiconductor standards. The degree of non-stoichiometry in thin films will depend mainly on the conditions of deposition as is discussed below.

2.2. Line Defects

The non-centrosymmetry of the sphalerite structure means that, corresponding to most of the simple geometrical types of dislocations in the diamond structure [26], there are two in the sphalerite structure [27]. For example, if both black and white atoms in fig. 3 are of the same chemical element, this is the 60° dislocation in the diamond structure. If the black circles represent A atoms, i.e. atoms of the lower valence element in the compound (e.g. III-valent atoms in a III-V compound), all the atoms with broken bonds along the dislocation line are of this element. Fig. 3 then represents an α 60° dislocation in the compound. Conversely, if the black circles represent B atoms, all the broken bonds dangle from atoms of the higher valence element, and fig. 3 represents a β 60° dislocation.

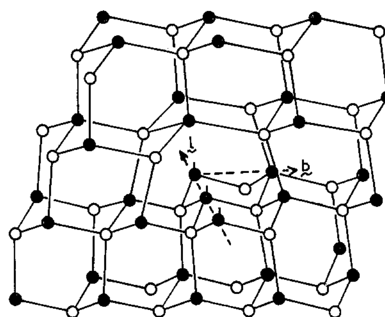

Figure 3 The 60° dislocation in the sphalerite structure. **l** and **b** lie along <110> directions. The slip plane is of {111} type. (Reproduced, by permission, from *J. Phys. Chem. Solids* [27].)

2.3. Two-Dimensional Defects

2.3.1. Grain Boundaries

The absence of a centre of symmetry means that there are four electrically-significant bonding errors that can occur in grain boundaries in the compounds. These are α dangling bonds, β dangling bonds, wrong A-A bonds, and wrong B-B bonds. In the diamond structure, however, only one occurs – the dangling bond. Geometrical analysis of $<110>$ and $<100>$ tilt boundaries in the sphalerite structure [28-

30] shows that boundaries can occur which contain the following combinations of bond errors: (i) wrong bonds all of one kind; (ii) equal numbers of both kinds of wrong bonds; (iii) wrong and broken bonds all of the same kind; and (iv) equal numbers of both kinds of broken bonds.

A particular case of special interest in connexion with epitaxy is the coherent {111} twin boundary in the diamond structure. Two geometrically different boundaries in the sphalerite structure, shown in fig. 4, correspond to the

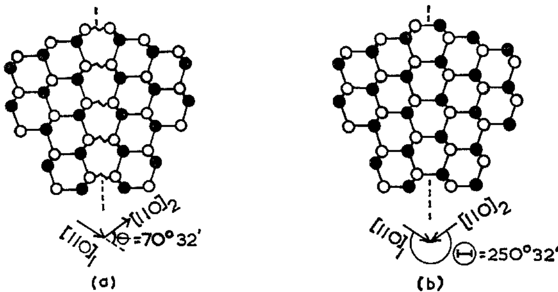

Figure 4 The boundaries resulting from tilts about the < 110 > axis of: (a) $\theta = 70° 32'$; (b) $\Theta = 250° 32'$. The Θ boundary is identical with the (111) boundary formed by a 60° twist about the [$1\bar{1}1$] axis. It is the commonly observed coherent ortho-twin boundary. It is not in the Θ-type but in the θ-type boundary that the grains are mirror-image related, however. The zig-zag lines represent wrong bonds in this and subsequent figures. (Reproduced, by permission, from *J. Phys. Chem. Solids* [30].)

single boundary in the diamond structure [30]. In the Θ-type or ortho-twin boundary, there are no wrong, broken, or strained bonds of any kind, so that this is a minimum energy boundary. In the θ-type or para-twin boundary, all the cross boundary bonds are wrong bonds of the same kind, so there are two forms, α and β, of this boundary. Such a twin can grow in thickness, in a direction perpendicular to the {111} interface, by the passage of a partial dislocation over each succeeding double {111} atomic plane. In this connexion, the partials are called twinning dislocations. In the θ case, the twinning dislocations contain no wrong bonds (see the discussion of fig. 5 below). The twinning dislocations in the Θ case, on the other hand, do contain wrong bonds (see fig. 5). Incoherent twin boundaries consist of arrays of twinning dislocations. The incoherent twin boundaries in ortho-twin (Θ) case will be of higher energy than the incoherent twin boundaries in the para-twin (θ) case. These energies are in the reverse order to that for the coherent twin boundaries of fig. 4. Such factors may lead to the occurrence of para-twins in epitaxial films.

2.3.2. Stacking Faults

Faults can be formed by aggregation of pairs of vacancies to remove a slab of material from a double {111} plane. The subsequent *inward* collapse of the lattice on either side produces an *intrinsic* stacking fault. Aggregation of pairs of interstitial atoms to form an *extra* slab of material in an out-of-sequence position between double {111} planes, and a consequent outward movement of the double atom planes on either side, to accommodate the slab, constitutes an *extrinsic* stacking fault. The dissociation of glide dislocations in the diamond and sphalerite structures can produce either intrinsic or extrinsic faults [31]. The mode of dissociation indicated in fig. 5a results in extrinsic faults, as for example in the form of the dissociated dislocation shown in fig. 5c. The mode of dissociation indicated in fig. 5b results in intrinsic faults, as for example in the form of the dissociated dislocation shown in fig. 5d.

There are four forms of dissociated 60° dislocation that are geometrically possible. They contain four types of stacking fault: (i) intrinsic *upright* faults (no wrong bonds up or down from the fault); (ii) intrinsic, *inverted* faults (wrong bonds up and down from the fault); (iii) extrinsic, upright faults; and (iv) intrinsic, inverted faults. The fault in fig. 5c is extrinsic and upright, and that in fig. 5d is intrinsic and inverted. Upright faulting (no wrong bonds up or down from the fault) is associated with partial dislocations which contain wrong bands as can be seen in fig. 5d. Inverted faulting (wrong bands up and down from the fault) is associated with partial dislocations which do not contain wrong bonds, as can be seen in fig. 5c. This point is important in relation to twinning, as was mentioned above.

The vacancy aggregation mechanism cannot invert double atom layers, so only upright or ortho-intrinsic faults will result from this mechanism. Pairs of interstitial atoms could, geometrically, aggregate with polarity inverted relative to the rest of the crystal. The inverted, or para-extrinsic, stacking fault so formed would be of high energy, as all the bonds directed outward normally from the inserted slab would

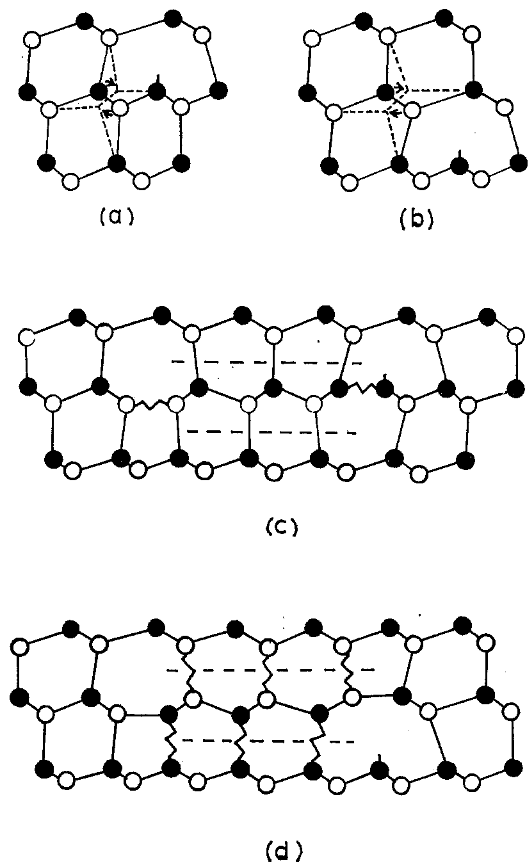

Figure 5 Geometrically possible modes of dissociation of a 60° dislocation in the sphalerite structure: (a) and (b) indicate two possible double atom ribbons which might rotate initially; (c) is the extended dislocation resulting from the rotation of the atom ribbon of (a) and its successors in the clockwise sense; (d) is the extended dislocation resulting from the rotation of the atom ribbon of (b) and succeeding ribbons in the anticlockwise sense. (Reproduced, by permission, from *J. Phys. Chem. Solids* [27].)

be wrong bonds. Thus, on energetic grounds, upright or ortho-extrinsic faults are to be expected to predominate.

It is also probable that, in certain materials at least, faulting will occur in complicated, regular or irregular arrays, corresponding not only to twinning but also to phase transformations [7, 8], including polytypic ones [2, 3], and to stacking disorder [10].

2.4. Heterojunction Misfit Dislocation Networks

Heterojunctions are interfaces between two different semiconducting materials. Their interest lies in that they are the sites of discontinuities of all the significant semiconductor parameters, and not just of charge carrier type as in the case of p-n junctions. Twenty-three different deposit/substrate pairs have been reported in the literature, counting only those involving the crystallographically related diamond-, sphalerite- and wurtzite-structure materials (for literature review see reference 32). When diamond- and sphalerite-structure materials grow epitaxially on each other, the lattice structure of the deposit will generally be a continuation of that of the substrate. The only change in the lattice across such an epitaxial interface is the parameter change.

The surface density of dangling bonds in the heterojunction is the difference between the numbers of bonds per unit area presented to the interface by the two materials [33], i.e.

$$\Delta N_S = N_{S1} - N_{S2} \qquad (1)$$

The number of bonds per unit area presented at the interface for any given heterojunction plane is given by

$$N_{S1,2} = \frac{n}{\mathbf{q}_1 \times \mathbf{q}_2} \qquad (2)$$

where $\mathbf{q}_1 \times \mathbf{q}_2$ is the unit mesh of the crystallographic plane, and n is the number of dangling bonds associated with this area. For example, fig. 6 shows the unit mesh for the (100) plane,

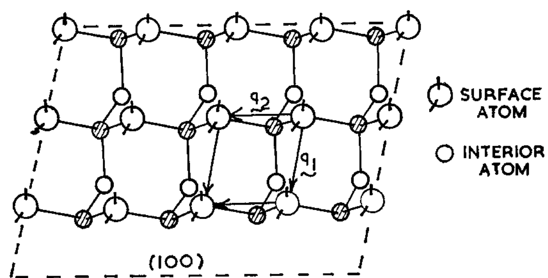

Figure 6 (100) surface of the sphalerite structure. Cross-hatched atoms are of one chemical species in the compound and open atoms are of the other species. $\mathbf{q}_1 = \lambda/2[0\bar{1}\bar{1}]$, $\mathbf{q}_2 = \lambda/2[0\bar{1}1]$. (Reproduced, by permission, from *J. Phys. Chem. Solids* [32].)

where $\mathbf{q}_1 = (\lambda/2)\ [0\bar{1}\bar{1}]$ and $\mathbf{q}_2 = (\lambda/2)\ [0\bar{1}1]$, so that the mesh area is $\mathbf{q}_1 \times \mathbf{q}_2 = \lambda^2/2$; where λ is the lattice parameter. At each corner of the mesh is an atom with two dangling bonds. The atom is at the meeting point of four similar parallelograms. Hence, $2/4 = \frac{1}{2}$ dangling bond per corner belongs to the mesh in question,

making a total of two bonds per mesh. The number of dangling bonds per unit area is therefore

$$N_{S1,2} = 2/\lambda^2/2 = 4/\lambda^2$$

The (1 1 0) and (1 1 1) planes may be dealt with similarly [32], leading via equation 1 to the results given in the third column of table I.

The dangling bonds will occur along the lines of the misfit dislocations which are required in an epitaxial interface (for a review see reference 34). These misfit dislocations accommodate the change of lattice parameter by constituting "extra half-planes" (actually double and triple atom-planes in these structures) in the material with the smaller lattice parameter.

The spacing of the misfit dislocations along any direction is given [34] by

$$p = ba/(b - a) \qquad (3)$$

where a is the repeat distance in the given direction in the material of the smaller lattice parameter, and b is the corresponding distance in the material of larger parameter. Values of p in microns for a number of practical cases are given in table I.

Pictures of the misfit dislocations may be constructed using ball and wire models, leading to results such as that shown in fig. 7a for the {1 1 1} heterojunction, with lattice parameters $7\lambda_2 = 8\lambda_1$. The cores of the dislocations contain three rows of atoms with dangling bonds [32], and the Burgers vectors are obtained on the RHLF convention, as indicated in fig. 7b and fig. 7c.

Proceeding in this way, the nature of the dislocations in each grid of any interface plane may be determined. The results for the (1 0 0), (1 1 0), and (1 1 1) planes are given in fig. 8a, b and c.

There are as yet no direct observations of heterojunction misfit dislocations in diamond- or sphalerite-structure materials. However, the geometry of diffusion-induced dislocations in p-n junctions is in principle the same as that of heterojunction misfit dislocations, and a number of observations of diffusion-induced dislocations have been reported. These observations, in general, confirm the results in fig. 8 (for a review see reference 32).

The numbers of dangling bonds per unit area in the heterojunctions (table I) are such as to

TABLE I Densities of dangling bonds and spacings of misfit dislocations in heterojunctions.

Heterojunction and lattice parameters (Å)	Plane	ΔN_S(cm^{-2})	p(μm)
Ge/GaAs	(1 0 0)	9.4×10^{12}	0.501
5.658/5.6535	(1 1 0)	6.7×10^{12}	$p_1 = 0.708$, $p_2 = 0.501$
	(1 1 1)	5.5×10^{12}	0.501
Ge/GaP	(1 0 0)	9.5×10^{13}	0.011
5.658/5.4506	(1 1 0)	6.8×10^{13}	$p_1 = 0.015$, $p_2 = 0.011$
	(1 1 1)	5.5×10^{13}	0.011
Ge/Si	(1 0 0)	1.1×10^{14}	0.010
5.658/5.431	(1 1 0)	7.5×10^{13}	$p_1 = 0.014$, $p_2 = 0.010$
	(1 1 1)	6.1×10^{13}	0.010
ZnS/Si	(1 0 0)	9.3×10^{12}	0.109
5.412/5.431	(1 1 0)	6.5×10^{12}	$p_1 = 0.155$, $p_2 = 0.109$
	(1 1 1)	5.4×10^{12}	0.109
ZnSe/GaAs	(1 0 0)	5.9×10^{12}	0.162
5.667/5.653	(1 1 0)	4.1×10^{12}	$p_1 = 0.229$, $p_2 = 0.162$
	(1 1 1)	3.4×10^{12}	0.162

p_1 and p_2 are the normal spacings of the $\mathbf{l}_1$, $\mathbf{b}_1$ and the $\mathbf{l}_2$, $\mathbf{b}_2$ dislocation grids in the (1 1 0) plane (see fig. 8b).

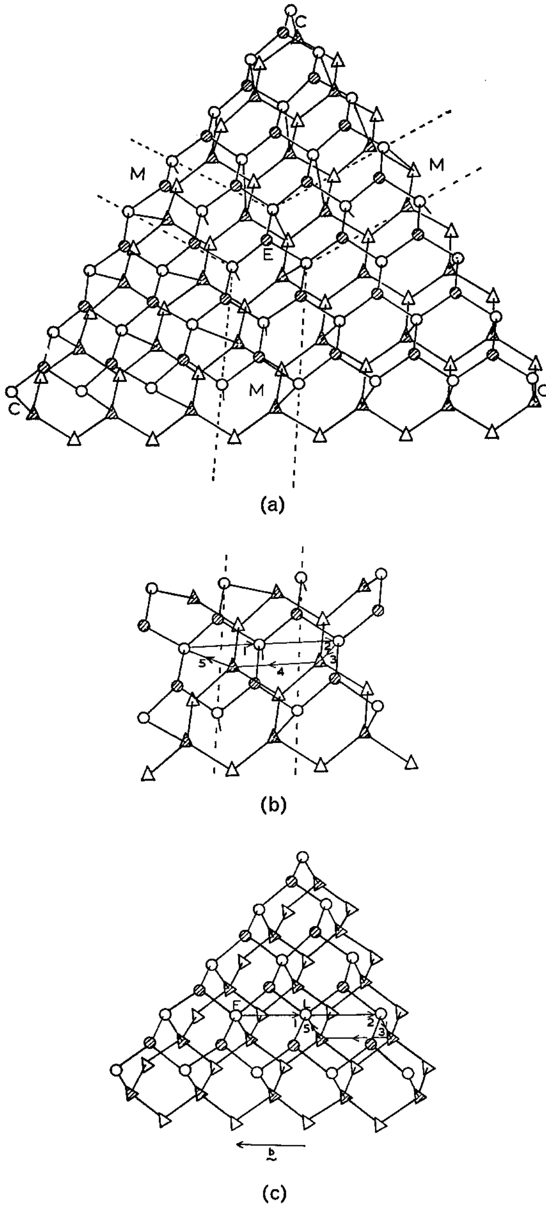

Figure 7 (a) {111} heterojunction between sphalerite structure crystals with lattice parameters $\lambda_1 = (7/8)\lambda_2$. The triple rows of atoms with dangling bonds indicated by broken lines constitute the cores of the dislocations. Circles are atoms in the upper (λ_1) crystal, triangles are atoms in the lower (λ_2) crystal. (b) Burgers circuit round a dislocation in the structure of (a). (c) Corresponding circuit in the perfect reference structure defining the Burgers vector by the RHLF convention. (Reproduced, by permission, from *J. Phys. Chem. Solids* [32].)

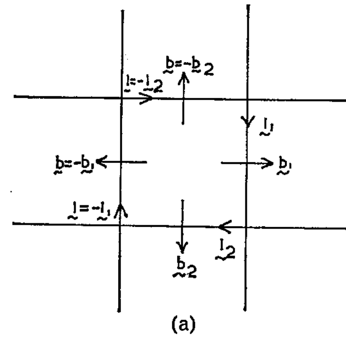

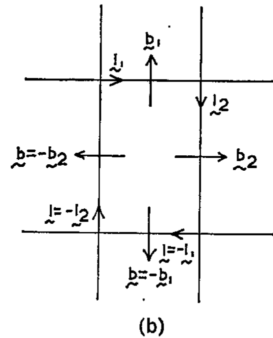

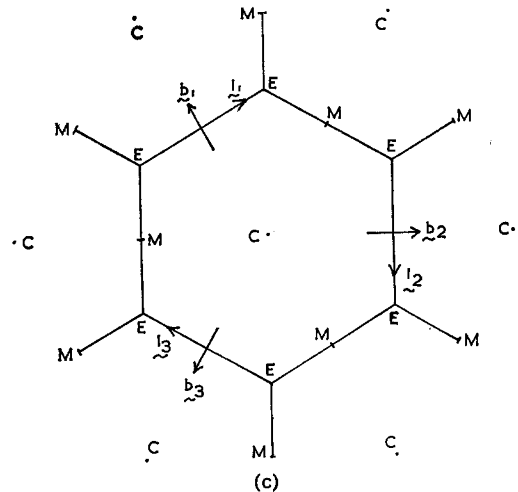

Figure 8 Dislocation arrays in heterojunction interfaces. (a) (100) plane: $\mathbf{l}_1 = [0\bar{1}\bar{1}]$ and $\mathbf{b}_1 = (\lambda_1 + \lambda_2)/4\ [01\bar{1}]$; $\mathbf{l}_2 = [0\bar{1}1]$ and $\mathbf{b}_2 = (\lambda_1 + \lambda_2)/4\ [0\bar{1}\bar{1}]$. (b) (110) plane: $\mathbf{l}_1 = [\bar{1}10]$ and $\mathbf{b}_1 = (\lambda_1 + \lambda_2)/2\ [001]$; $\mathbf{l}_2 = [00\bar{1}]$ and $\mathbf{b}_2 = (\lambda_1 + \lambda_2)/4\ [\bar{1}10]$. (c) (111) plane: $\mathbf{l}_1 = [\bar{2}11]$ and $\mathbf{b}_1 = (\lambda_1 + \lambda_2)/4\ [0\bar{1}1]$; $\mathbf{l}_2 = [11\bar{2}]$ and $\mathbf{b}_2 = (\lambda_1 + \lambda_2)/4\ [\bar{1}10]$; $\mathbf{l}_3 = [1\bar{2}1]$ and $\mathbf{b}_3 = (\lambda_1 + \lambda_2)/4\ [10\bar{1}]$. (Reproduced, by permission, from *J. Phys. Chem. Solids* [32].)

suggest that they may strongly influence the electrical properties of heterojunctions [33]. In particular, it is possible to explain in this way [32] the variation of barrier voltages in the sequence (111) Ga > $(\bar{1}\bar{1}\bar{1})$ As > (110) in n-n Ge/GaAs heterojunctions, and in the reverse sequence (110) > $(\bar{1}\bar{1}\bar{1})$ As > (111) Ga in n-p Ge/GaAs heterojunctions [35]. The reason

is that the α dangling bonds of the (111) Ga heterojunction will produce a larger surface charge than the β dangling bonds of the $(\bar{1}\bar{1}\bar{1})$ As heterojunction, or the equal numbers of α and β dangling bonds of the (110) heterojunction. The effect of superimposing the surface charges, as indicated in fig. 9b, as compared with fig. 9a, is to increase the barrier to current flow in the n-n heterojunctions. In the n-p heterojunctions, however, the superimposed surface charges decrease the effective barrier voltages, as indicated in fig. 9d compared with fig. 9c. The dangling bonds will also tend to pin the Fermi level near the middle of the forbidden energy gap, as it has been observed to be in Ge/GaP heterojunctions [36].

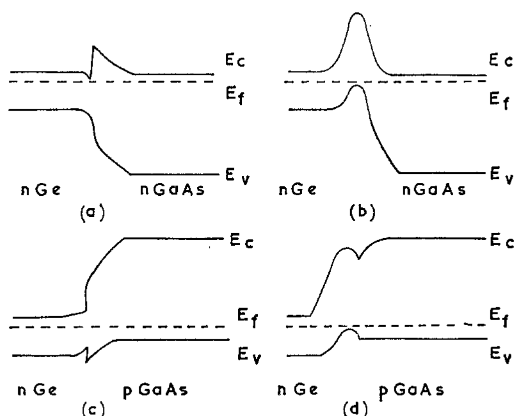

Figure 9 Schematic energy band diagrams of Ge/GaAs heterojunctions: (a) and (c) are the n-n and n-p junctions respectively (after Fang and Howard [35]); (b) n-n heterojunction with a large negative interface charge; (d) n-p heterojunction with a large negative interface charge. (Reproduced, by permission, from *J. Phys. Chem. Solids* [32].)

3. Experimental Studies of Epitaxial Films of Semiconducting Compounds

3.1. Methods for Depositing Films

Many of the sphalerite-structure compounds dissociate on heating in vacuum, so that the simple vacuum evaporation technique for film deposition cannot be used. A variety of methods for circumventing this difficulty are available including the following.

(a) *Flash evaporation* Fine particles of the compound are dribbled onto an evaporator held well above the sublimation temperature of the most refractory constituent, so that the whole of each particle flashes off the evaporator simultaneously and before the next particle arrives [37-39]. This ensures stoichiometric evaporation. If the sticking coefficients of the constituents of the vapour on the substrate are equal, or if a self-balancing tendency exists owing to a large formation energy of the compound, a comparatively stoichiometric deposit will result. In practice, approximately stoichiometric deposits are often obtained.

(b) *Disproportionation and other chemical transport reactions* Many techniques of this type have been developed. For example, III-V compounds have been deposited by using HCl [40], iodine [41], and water vapour [42] as transporting agents. Here, control of the chemical variables is used to produce approximate stoichiometry and also doping when this is required.

(c) *Sputtering* [43] can also be used to produce approximately stoichiometric films.

(d) *The three-temperature method* [44] in which the elements, A and B, that make up the compound are separately evaporated from sources at temperatures T_1 and T_2 onto a substrate at temperature T_3. Temperatures T_1 and T_2 and the apparatus geometry are so arranged that the rate of arrival at the substrate surface of atoms of the more volatile constituent is two to ten times as great as that of atoms of the other constituent. The substrate temperature is so chosen that the sticking coefficients of the two constituents differ, and approximately equal numbers of A and B atoms are deposited. This technique has been shown to result in films of III-V compounds of comparatively good electrical properties, but no structural studies have been made.

(e) *Use of semiconducting compounds which do not dissociate appreciably on sublimation* (that is, not to an extent detectable by electron diffraction). These are chiefly the II-VI compounds.

Despite the adoption of experimental techniques to minimise it, some degree of non-stoichiometry must be expected to be present in any real film of a compound. Comparatively small deviations from stoichiometry must be expected to have a large influence on electrical properties, as was pointed out in section 2.1. Nevertheless, comparatively little attention has been devoted to the problem of non-stoichiometry. This is largely due to the lack of experimental techniques for its measurement in thin films. Conclusions about the stoichiometry of films are usually drawn either from electrical

measurements or from electron diffraction observations. However, it is difficult to disentangle the effects of non-stoichiometry on electrical properties from those of impurity contamination and crystalline defects. Electron diffraction data, as obtained in electron microscopes, lack sufficient sensitivity to detect the small deviations from stoichiometry which are important for semiconductor properties, and few laboratories have precision electron diffraction cameras available for thin film work.

3.2. The Variation of Film Structure with Substrate Temperature

CdTe films evaporated in vacuum onto mica substrates at a series of increasing temperatures were examined by transmission electron microscopy by Suito and Shiojiri [45], with the result given in fig. 10. The characteristic feature of such sequences is that as the temperature increased the grain size in the films increased, and the diffraction patterns changed from randomly-oriented ring patterns (fig. 10b) to well-oriented spot patterns (fig. 10h). Similar sequences of diffraction patterns have been observed in many other cases, including that of GaAs sputtered onto NaCl [46]. Ino, Watanabe, and Ogawa [47] introduced a parameter, R, which has the values: $R = 0$, for ring patterns; $R = 25$, for mixed patterns in which the ring pattern predominates; $R = 50$, when ring and spot patterns are equally prominent; $R = 75$, for mixed patterns in which the spot pattern predominates; and $R = 100$, for a spot pattern alone. Ino *et al* consider R to be proportional to the percentage of oriented material in the film.

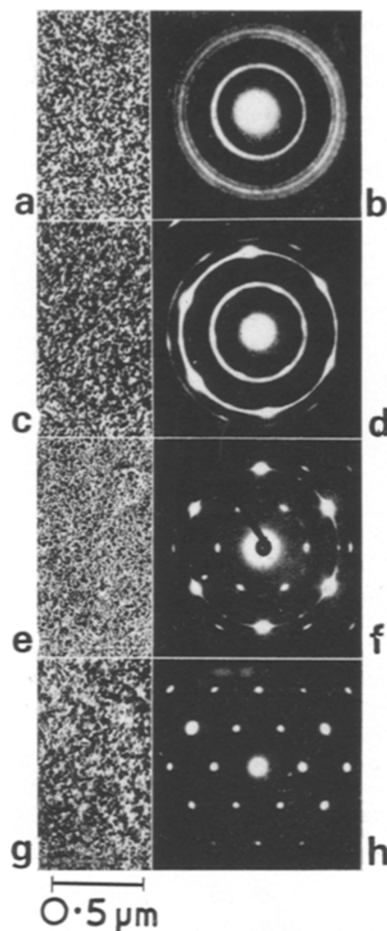

Figure 10 Electron micrographs and electron diffraction patterns of CdTe films deposited on mica substrates, the temperatures of which were 20° C in (a) and (b); 150° C in (c) and (d); 250° C in (e) and (f); and 350° C in (g) and (h). (Reproduced, by permission, from *J. Electronmicroscopy* [45].)

By recording R values and measured grain sizes, the development of film structure with substrate temperature can be represented graphically as in fig. 11a and b, for the case of ZnTe evaporated onto (100) cleavage faces of NaF in vacua in the 10^{-5} torr range [48]. ZnTe films evaporated onto the (100) cleavage faces of NaCl and LiF give graphs similar to fig. 11.

A number of important items of diffraction information are not disclosed by the R values however. For example, tilting reveals the presence of a fibre texture in films in the upper part of the $R = 0$ temperature range. That is, before the R values begin increasing, the grains in the films are no longer randomly oriented with respect to two of the three rotational degrees of freedom. As the fibre texture develops, the grains tend to have a particular crystallographic axis [100], perpendicular to the substrate face (100). They remain randomly oriented in azimuth about this direction, however. The rise of the R values at higher temperatures means that more and more grains have certain low-energy azimuthal positions. When they all have the same azimuthal position, epitaxy results.

Thus, the films formed at the lowest temperatures consist of small volumes randomly oriented. At higher temperatures, the individual grains are larger and randomly oriented only about the substrate face normal. With further

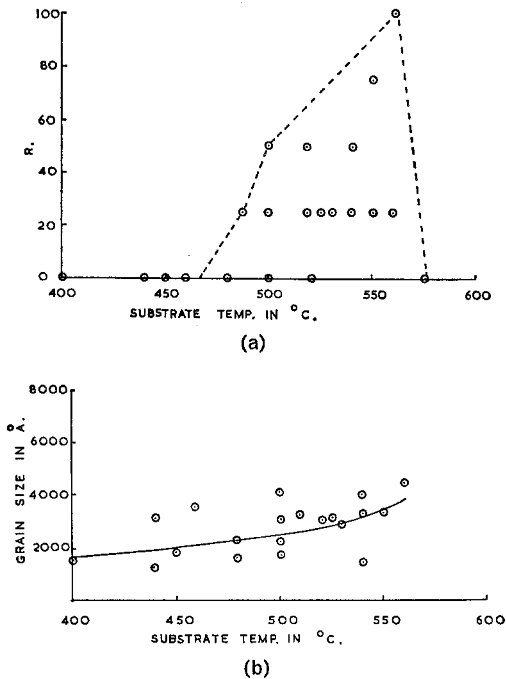

Figure 11 (a) Values of R (degrees of orientation) of a number of ZnTe/NaF films as a function of substrate temperature. (b) Grain size in the films as a function of temperature.

increase in temperature, the grains increase in size, and an increasing fraction of them is found in the epitaxial or multiply positioned low-energy azimuthal positions. Twinning about the substrate face normal is one possible form of multiple positioning (double positioning [1]).

In the CdTe/mica [45], ZnTe/NaCl, ZnTe/NaF and ZnTe/LiF [48], and InSb/mica [39] cases, films are obtained which look fine-grained in the electron microscope, but give rise to electron diffraction spot patterns. This arises because of the difference in orientation-sensitivity of the two kinds of observation. Two areas will appear in differing contrast on an electron micrograph if they differ in orientation by an angle of the order of a tenth of a degree. To give rise to resolved spots on the diffraction pattern however, two grains must be misoriented by several degrees.

Epitaxial growth of ZnTe on NaCl, NaF, and LiF is poor, both because there is no reproducibility in R values at the optimum temperature (fig. 11a), and because even $R = 100$ films remain polycrystalline, although the grain boundary misorientations are less than 2 to 3°.

ZnTe grows epitaxially on the (111) cleavage faces of CaF_2, in the manner indicated in fig. 12. In this case, there is a wide range of temperatures (fig. 12a) over which $R = 100$ films are formed reproducibly, and these films appear monocrystalline, as can be seen in fig. 13b, but contain numbers of small included grains and stacking faults. The average lengths of the included grains (twins) and stacking faults are plotted as the dotted curve in fig. 12b. Growth of ZnTe on BaF_2 occurs in a similar fashion to that shown in fig. 12. CdSe vacuum evaporated onto mica grows similarly to ZnTe on BaF_2 and CaF_2 (I. Brunnschweiler, private communication).

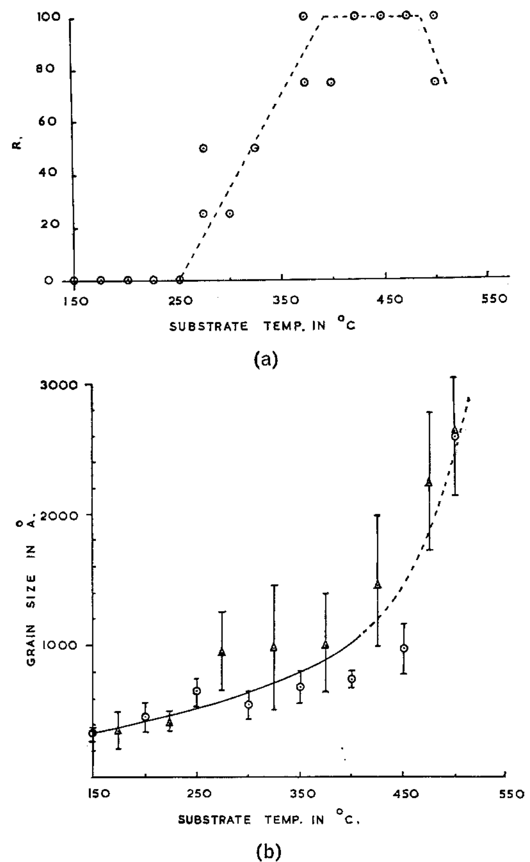

Figure 12 (a) R versus substrate temperature for ZnTe films evaporated onto (111) CaF_2 in vacuum. (b) Grain size versus temperature for ZnTe/CaF_2 films.

3.3. Microtwins and Wurtzite

The diffraction patterns from the epitaxial ZnTe/BaF_2 films contain a multitude of "irrational", satellite spots [48], as can be seen in fig. 13a. Satellite spots have also been observed in reflection electron diffraction patterns from GaP, GaAs, GaSb, InP, InAs, InSb, and AlSb

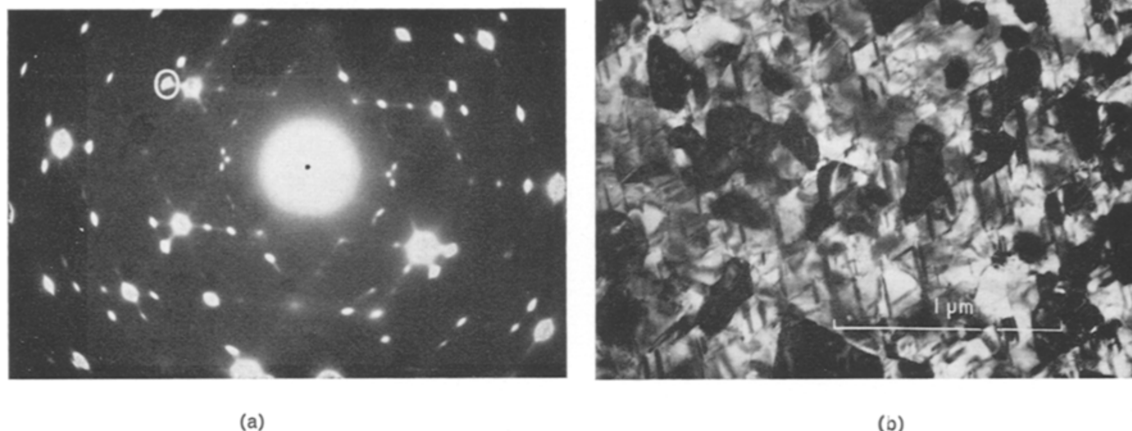

(a) (b)

Figure 13 Epitaxial film of ZnTe evaporated in vacuum onto (1 1 1) CaF_2 at 450° C. (a) Diffraction pattern and (b) electron micrograph.

flash-evaporated in vacuum onto Ge. The irrational spots in these cases were interpreted as indicating twinning. Temperatures were listed for onset of oriented growth ($R > 0$), "epitaxy with twinning" and "untwinned epitaxy" [37, 38]. Sputtered GaAs films on Ge also gave rise to satellite spots in reflection electron diffraction patterns, which were attributed to twinning [43]. A detailed interpretation of satellite spots in GaAs films deposited onto Ge by HCl transport [49] led to two conclusions. Firstly, that both first and higher order twins, i.e. twin orientations which are equivalent to successive twinning about more than one <1 1 1> axis, were present in the films. Secondly, that the deposition temperatures required for the elimination of twinning increase with substrate orientation in the order $\{001\} < \{110\} < \{111\}$.

The satellite spots in (1 1 1)-oriented epitaxial films of CdTe prepared by vacuum evaporation onto mica were interpreted by Shiojiri and Suito [50] as being due to the presence of twins and of wurtzite-structure material on each of the {1 1 1} planes, as indicated in fig. 14. This structure would give rise to the array of spots in fig. 15 and is a possible interpretation of the diffraction patterns obtained by Shiojiri and Suito. Electron diffraction evidence has also been interpreted by several Russian workers as indicating the presence of both cubic and hexagonal phases in epitaxial films of a number of II-VI compounds [51-59]. These studies are listed in table II. It has been reported also that both wurtzite and

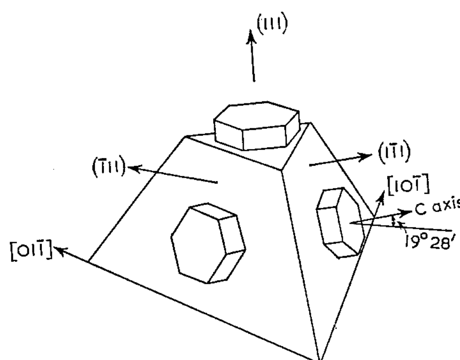

Figure 14 Schematic diagram of the lattice orientations of hexagonal wurtzite-structure crystallites in an epitaxial film with (1 1 1) orientation. (Reproduced, by permission, from *Japan. J. Appl. Phys.* [50].)

sphalerite structures were present in films of CdS evaporated onto glass [60], but later X-ray analysis of CdS evaporated onto mica and onto molybdenum emphasised the difficulty of structure analysis, since most wurtzite and sphalerite diffraction rings coincide within experimental error [61].

An alternative interpretation has been overlooked in all the analyses listed in table II and in the work of Shiojiri and Suito [50]. It is difficult to distinguish between spots or rings owing to hexagonal phase material in a cubic matrix, and spots or rings due to double diffraction first in cubic material and then in twinned cubic material. Twin-matrix double electron diffraction is known to be important in epitaxial

TABLE II Reported structures of epitaxial films of semiconducting compounds.

Deposit and substrate	Deposition	Substrate temperatures (° C)	Structure	Method of observation	Reference
CdTe on NaCl or mica	Vacuum sublimation	Room temperature to 300	"Cubic and hexagonal" (sphalerite and wurtzite)	Transmission electron diffraction	51
CdS, CdSe, and CdTe on NaCl and mica	,,	200 to 300	Cubic and hexagonal with stacking faults	,,	52
InSb on NaCl	,,		Sphalerite and wurtzite structure	,,	53
CdSe on (1 1 1) NaCl, KCl, and KBr	,,	20 to 250 At 250	$R = 0 \rightarrow R = 100$ Hexagonal + "irrational reflection bands"	,,	54
CdTe on NaCl and mica	,,	200 to 300	Cubic and hexagonal	,,	55
CdSe on (1 0 0) and (1 1 0) faces of NaCl	,,	Room temperature	Hexagonal polycrystalline	,,	56
		250 to 350	Cubic + hexagonal		
CdTe on NaCl, KCl, and KBr	,,	?	Cubic + hexagonal + twinned cubic	,,	57
InSb on mica	Vacuum flash evaporation	320 to 455	Cubic + hexagonal (+ stacking faults in thick films). Grain size increased with substrate temperature	,,	58
ZnSe and CdSe on (1 1 1) NaCl and ZnSe on CdSe on (1 1 1) NaCl	Vacuum evaporation	250 to 350	Cubic, hexagonal or mixed depending on deposition conditions	Reflection and transmission electron diffraction	59

films of fcc metals, and has on occasion led to erroneous interpretations of film structure in terms of the presence of both cubic and hexagonal material [1, 62-64]. Since this possibility has not been considered or tested in the work listed in table II, nor in the work of Shiojiri and Suito [50], the structures reported in these papers must be regarded as unproved.

Evidence that double diffraction contributes to the diffraction pattern from $ZnTe/CaF_2$ films is provided by fig. 16. The interpretation of fig. 16 is given in fig. 17. It will be seen that it is indeed the larger twins which appear in outline only, whereas the narrower ones are uniformly bright.

3.4. The Effect of Vapour Composition and Substrate Structure on Film Structure

Further ground for extreme caution in interpretation is given by a report that ZnTe, vacuum evaporated onto glass, is cubic, while co-evaporation of ZnTe and metallic Zn results in films containing both cubic and hexagonal ZnTe [65]. Similarly, it is found that it is possible to predetermine which SiC polytype is deposited by controlling the ratio of the components fed into the system in a chemical reaction technique. (R. P. Sutton and J. G. Wilkes, private communication.) It has also been reported that, in the case of vapour phase isoepitaxial growth of GaAs, excess Ga in the vapour phase suppresses growth on the Ga (1 1 1) face and promotes growth on the As $(\bar{1}\bar{1}\bar{1})$ face. Conversely, excess As in the vapour phase suppresses growth on the As $(\bar{1}\bar{1}\bar{1})$ face and speeds up growth on the Ga (1 1 1) face. Moreover, small variations in the Ga:As ratio

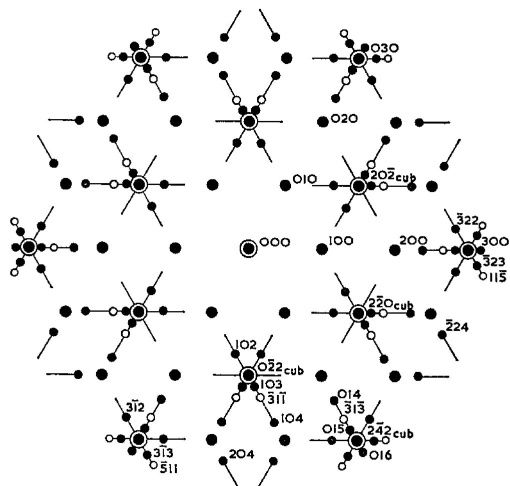

Figure 15 Array of diffraction spots arising from the structure of fig. 14. O spots due to cubic material with (1 1 1) plane parallel to the film plane; ● extra spots due to wurtzite grains with the basal plane parallel to the (1 1 1) plane in the cubic matrix; ● due to wurtzite grains with the basal parallel to the ($\bar{1}$11), (1$\bar{1}$1) and (11$\bar{1}$) planes of the matrix; o spots due to sphalerite microtwins with twinning planes parallel to the ($\bar{1}$11), (1$\bar{1}$1) and (11$\bar{1}$) planes in the matrix. (Reproduced, by permission, from *Japan. J. Appl. Phys.* [50].)

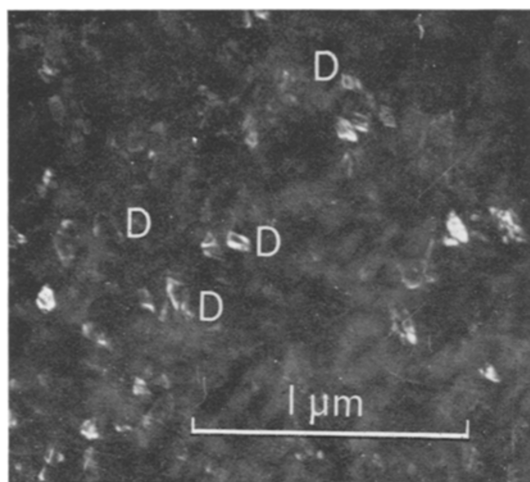

Figure 16 ZnTe/CaF_2 dark field micrograph using the satellite spot ringed in fig. 13a. Double diffraction images are marked D.

were found to alter greatly the defect content and surface topography of the deposited layers [66].

These observations may all represent evidence for the influence of non-stoichiometry on structure. However, it is difficult to disentangle the

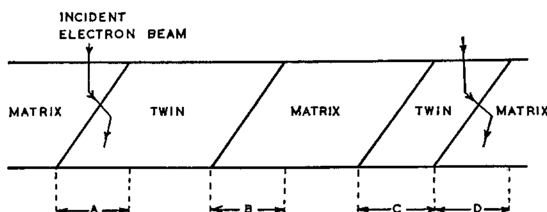

Figure 17 The areas in which matrix/twin double diffraction can occur, as at A, are at the boundaries of microtwins. If the twin is wide, the boundaries will be resolved as at A and B, but narrow twins will appear uniformly illuminated in dark field as at C and D.

influence of the numerous growth parameters in the case of chemical deposition techniques. For example, in the epitaxial growth of GaAs using As and Ga, orientation dependent contamination decreases the perfection of deposits grown on As faces much more than that of deposits grown on Ga faces. (H. Holloway, private communication.) Moreover, in the case of both the iodine and the chloride deposition systems, the ratio of the growth rate on the Ga face to the growth rate on the As face decreases with increasing concentrations of the lower halide in the gas stream [67].

A further factor which may influence the crystal structure of the deposit is the structure of the substrate. Thus, it has been reported that CdTe grows on wurtzite-structure CdS with an hexagonal structure like the substrate, rather than with the cubic structure in which CdTe normally crystallises. Similarly, CdS reportedly grew in "metastable, rhombohedral, or 3R (sphalerite-type)" modifications on the ($\bar{1}\bar{1}\bar{1}$) P face of GaP, but grew in its normal hexagonal form on the (1 1 1) Ga face of GaP [68].

It cannot, therefore, be assumed that the structure found in an epitaxial film produced under one set of circumstances will recur under different experimental conditions. It is clear that all the available electron microscope diffraction contrast techniques, as well as electron diffraction analysis, will be needed in order to establish unequivocally, and in detail, the structure of epitaxial films of semiconducting compounds.

3.5. Stacking Faults and Dislocations

GaAs films produced by vapour phase techniques have been examined by optical microscopy both in the as-grown condition [69] and after etching

[70]. Triangular defects were found which may be similar to the well-known stacking fault tetrahedra in Si [1]. GaP films vapour deposited on GaAs have been found, after etching, to contain pits and etch channels which have been interpreted as indicating the presence of dislocations, stacking faults, and impurity striae. It was found that the stacking faults could be eliminated by growing on $(\bar{1}\bar{1}\bar{1})$ As substrate faces under carefully controlled conditions [71].

Stacking faults, dislocations, and dislocation networks appear in vacuum-evaporated ZnTe/CaF_2 films [48], as can be seen in fig. 18. The

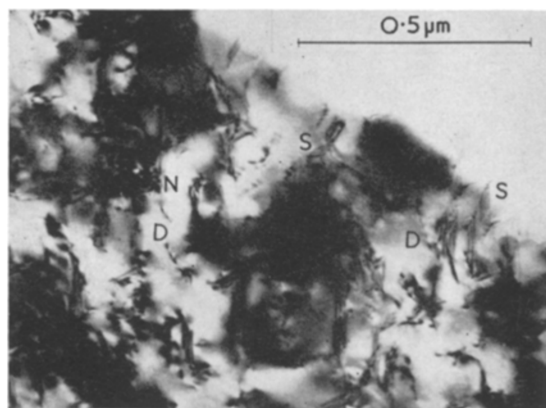

Figure 18 Defects in an epitaxial film of ZnTe grown on CaF_2. At S are stacking faults, at D are dislocations, and at N a dislocation network.

densities of both stacking faults and dislocations are in the range from 10^9 to $10^{10}/cm^2$.

No identifications of dislocation or stacking fault types have yet been reported in epitaxial films of semiconducting compounds. Methods have been developed for such identification by workers studying bulk material, however. Methods for identification of dislocation type (α or β) include etching [72, 73] and diffraction contrast methods for determining the sense of Burgers vectors (reference 64 pp. 14, 15 and 263-265). The determination of the sense of the Burgers vector makes it possible to identify the chemical (α or β) type of a dislocation, if, in addition, the polarity of the specimen is determined, i.e. whether, for example, the top of the specimen is an A (1 1 1) surface (consisting of the lower valence atoms only) and the bottom a B $(\bar{1}\bar{1}\bar{1})$ surface (consisting of the higher valence atoms only), or vice versa. This procedure has thus far only been applied to InSb, using the Lang technique of X-ray projection topography. (A. R. Lang, private communication.) (The Lang technique has also been used to observe dislocations in SiC of polytype 6H structure and to determine their Burgers vectors and line directions [74].) Similarly, diffraction contrast techniques make possible determinations of stacking fault Burgers vectors. Observations of stacking faults using transmission electron microscopy on wurtzite-structure crystals, which were thin enough, as grown, to be electron transparent, have been reported in the cases of ZnS [75-80], CdS [77, 81-83], and AlN [75, 84-86]. Details of the diffraction contrast method for determining fault vectors in the wurtzite structure are given in three of these papers [80, 85, 86]. The application of these techniques to sphalerite-structure material and to epitaxial films would be comparatively straightforward and make possible detailed analysis of the defect content of the films.

4. Conclusions

In compounds with the sphalerite structure, two or more types of defects are geometrically possible, corresponding to each type of defect in the diamond-structure elements. This greater complexity is due to the absence of a centre of symmetry in the sphalerite structure. In addition, there is the possibility of the occurrence of many regular and irregular stacking sequences, besides the sequence corresponding to the sphalerite structure.

The expectation that the structural defects in epitaxial films of sphalerite-structure compounds will be broadly similar to those found in films of fcc and diamond-structure materials is borne out by the electron diffraction studies of films of seven III-V compounds and of five II-VI compounds. Transmission electron microscopy is beginning to be applied to the problem, making possible detailed analysis of the types of defects present in epitaxial films of these materials.

Acknowledgements

It is a pleasure to thank Professor J. G. Ball for the provision of research facilities, and the Ministry of Defence (Navy Department) for financial support.

References

1. D. W. PASHLEY, *Adv. in Phys.* **14** (1965) 327.
2. W. F. KNIPPENBURG, *Philips Res. Repts.* **18** (1963) 161.

3. C. FRONDEL and C. PALACHE, *Am. Mineral.* **35** (1950) 29.
4. L. W. STROCK and V. A. BROPHY, *Am. Mineral.* **40** (1955) 94.
5. A. S. PASHINKIN, G. N. TISHCHENKO, I. V. KORNEEVA, and B. N. RYZHENKO, *Sov. Phys. Cryst.* **5** (1960) 243.
6. F. SCHOSSBERGER, *J. Electrochem. Soc.* **102** (1955) 22.
7. D. C. BUCK and L. A. STROCK, *Am. Mineral.* **40** (1955) 192.
8. H. BLANK, P. DELAVIGNETTE, R. GEVERS, and S. AMELINCKX, *Phys. Stat. Sol.* **7** (1964) 747.
9. D. B. HOLT, to be published.
10. T. PETERS, J. SINGER, V. A. BROPHY, and J. L. BIRMAN, *J. Appl. Phys.* **34** (1963) 2210.
11. R. A. SWALIN, *J. Phys. Chem. Solids* **18** (1961) 290.
12. A. SCHOLZ, *Phys. Stat. Sol.* **3** (1963) 42.
13. A. SCHOLZ and A. SEEGER, *Phys. Stat. Sol.* **3** (1963) 1480.
14. S. ASANO and Y. TOMISHIMA, *J. Phys. Soc. Japan* **13** (1958) 1119 and 1126.
15. R. J. HODGKINSON, *J. Electronics* **1** (1955-56) 612.
16. R. J. HODGKINSON, *J. Electronics* **2** (1956-57) 201.
17. R. F. BREBICK, *J. Phys. Chem. Solids* **11** (1959) 43.
18. M. E. STRAUMANIS and C. D. KIM, *Acta Cryst.* **19** (1965) 256.
19. B. K. CHAKRAVERTY and R. W. DREYFUS, *J. Appl. Phys.* **37** (1966) 631.
20. B. GOLDSTEIN and N. ALMELEH, *Appl. Phys. Letters* **2** (1963) 130.
21. C. S. FULLER and K. B. WOLFSTIRN, *J. Appl. Phys.* **33** (1962) 745.
22. C. S. FULLER and K. B. WOLFSTIRN, *J. Appl. Phys.* **33** (1962) 2507.
23. C. S. FULLER and K. B. WOLFSTIRN, *J. Appl. Phys.* **34** (1963) 1914.
24. J. BLANC, R. H. BUBE, and L. R. WEISBERG, *J. Phys. Chem. Solids* **25** (1964) 225.
25. J. C. BRICE and G. D. KING, *Nature* **209** (1966) 1346.
26. J. HORNSTRA, *J. Phys. Chem. Solids* **5** (1958) 129.
27. D. B. HOLT, *J. Phys. Chem. Solids* **23** (1962) 1353.
28. J. HORNSTRA, *Physica* **25** (1959) 409.
29. J. HORNSTRA, *Physica* **26** (1960) 198.
30. D. B. HOLT, *J. Phys. Chem. Solids* **25** (1964) 1385.
31. S. AMELINCKX, "The Direct Observation of Dislocations", Solid State Physics, Supplement 6 (Academic Press, New York, 1964), pp. 278-280.
32. D. B. HOLT, *J. Phys. Chem. Solids* **27** (1966) 1053.
33. W. G. OLDHAM and A. G. MILNES, *Solid State Electronics* **7** (1964) 153.
34. J. H. VAN DER MERWE, "Single Crystal Films" (Pergamon Press, Oxford, 1964), p. 139.
35. F. F. FANG and W. E. HOWARD, *J. Appl. Phys.* **35** (1964) 612.
36. L. J. VAN RUYVEN, J. M. P. PAPENHUIZEN, and A. C. J. VERHOEVEN, *Solid State Electronics* **8** (1965) 631.
37. J. L. RICHARDS, P. B. HART, and L. M. GALLONE, *J. Appl. Phys.* **34** (1963) 3418.
38. J. L. RICHARDS, P. B. HART, and E. K. MULLER, "Single-Crystal Films" (Pergamon Press, Oxford, 1964), p. 241.
39. C. JUHASZ and J. C. ANDERSON, *Phys. Letters* **12** (1964) 163.
40. R. R. MOEST and B. R. SHUPP, *J. Electrochem. Soc.* **109** (1962) 1061.
41. S. M. KU, *J. Electrochem. Soc.* **110** (1963) 991.
42. G. E. GOTTLIEB, *J. Electrochem. Soc.* **112** (1965) 192.
43. B. MOLNAR, J. J. FLOOD, and M. H. FRANCOMBE, *J. Appl. Phys.* **35** (1964) 3554.
44. K. G. GUNTHER, "Compound Semiconductors", edited by R. K. Willardson and H. L. Goering (Reinhold, New York, 1962), p. 313.
45. E. SUITO and M. SHIOJIRI, *J. Electronmicroscopy* **12** (1963) 134.
46 T. EVANS and A. J. NOREIKA, *Phil. Mag.* **13** (1966) 717.
47. S. INO, D. WATANABE, and S. OGAWA, *J. Phys. Soc. Japan* **19** (1964) 881.
48. D. B. HOLT, to be published.
49. H HOLLOWAY, K. WOLLMANN, and A. S. JOSEPH, *Phil. Mag.* **11** (1965) 263.
50. M. SHIOJIRI and E. SUITO, *Japan. J. Appl. Phys.* **3** (1964) 314.
51. S. A. SEMILETOV, *Trudy. Inst. Krist. Nauk. SSSR* **11** (1955) 121.
52. S. A. SEMILETOV, *Kristollografiya* **1** (1956) 306.
53. S. A. SEMILETOV, *Sov. Phys. Cryst.* **2** (1957) 281.
54. I. P. KALINKIN, L. A. SERGEEVA, V. B. ALESKOVSKII, and L. P. STRAKHOV, *Sov. Phys. Sol. State* **3** (1962) 1922.
55. M. A. RUMSH, F. T. NOVIK, and T. M. ZIMKINA, *Sov. Phys. Cryst.* **7** (1963) 711.
56. I. P. KALINKIN, L. A. SERGIEVA, V. B. ALESKOVSKII, and L. P. STRAKHOV, *Sov. Phys. Sol. State* **5** (1963) 86.
57. F. T. NOVIK, M. A. RUMSH, and T. M. ZIMKINA, *Sov. Phys. Cryst.* **8** (1963) 295.
58. S. A. SEMILETOV and P. S. AGALARZADE, *Sov. Phys. Cryst.* **9** (1965) 409.
59. L. A. SERGEEVA, I. P. KALINKIN, and V. B. ALESKOVSKII, *Sov. Phys. Cryst.* **10** (1965) 178.
60. P. H. WENDLAND, *J. Opt. Soc. Am.* **52** (1962) 581.
61. C. A. ESCOFFERY, *J. Appl. Phys.* **35** (1964) 2273.
62. D. W. PASHLEY and M. J. STOWELL, *Phil Mag.* **8** (1963) 1605.
63. D. W. PASHLEY, M. J. STOWELL, and T. J. LAW, *Phys. Stat. Sol.* **10** (1965) 153.
64. P. B. HIRSCH, A. HOWIE, R. B. NICHOLSON, D. W. PASHLEY, and M. J. WHELAN, "Electron Microscopy of Thin Crystals" (Butterworths, London, 1965), p. 148.
65. K. V. SHALIMOVA, A. F. ANDRUSHKO, I. SPYNULESKU-KARNARU, and B. P. SEREDINSKII, *Sov. Phys. Cryst.* **9** (1965) 623.

66. R. E. EWING and P. E. GREENE, *J. Electrochem. Soc.* **111** (1964) 1266.
67. N. GOLDSMITH, *J. Electrochem. Soc.* **110** (1963) 588.
68. M. WEINSTEIN, G. A. WOLFF, and B. N. DAS, *Appl. Phys. Letters* **6** (1965) 73.
69. J. A. AMICK, "Single-Crystal Films" (Pergamon Press, Oxford, 1964), p. 283.
70. A. ITO, M. ISHII, and M. ITO, *Phys. Abstracts* 5=6395 (1965), originally reported in *Mitsubishi Denki Lab. Rep.* (Japan) **5** (1964) 501.
71. W. G. OLDHAM, *J. Appl. Phys.* **36** (1965) 2887.
72. R. L. BELL and A. F. W. WILLOUGHBY, *J. Matls. Sci.* **1** (1966) 219.
73. H. C. GATOS and M. C. LAVINE, *Prog. Semicond.* **9** (1964) 1.
74. S. AMELINCKX, G. STRUMANE, and W. W. WEBB, *J. Appl. Phys.* **31** (1960) 1359.
75. J. BLANK, P. DELAVIGNETTE, and S. AMELINCKX, *Phys. Stat. Sol.* **2** (1962) 1660.
76. L. T. CHADDERTON, A. G. FITZGERALD, and A. D. YOFFE, *J. Phys. Chem. Solids* **24** (1963) 592.
77. L. T. CHADDERTON, A. G. FITZGERALD, and A. D. YOFFE, *Nature* **198** (1963) 573.
78. L. T. CHADDERTON, A. G. FITZGERALD, and A. D. YOFFE, *Phil Mag.* **8** (1963) 167.
79. L. T. CHADDERTON, A. G. FITZGERALD, and A. D. YOFFE, *J. Appl. Phys.* **35** (1964) 1582.
80. H. BLANK, P. DELAVIGNETTE, R. GEVERS, and S. AMELINCKX, *Phys. Stat. Sol.* **7** (1964) 747.
81. W. MOHLING, H. PEIBST, and L. HILDISCH, *Phys. Stat. Sol.* **5** (1964) 101.
82. W. MOHLING and J. HEYDENREICH, *Phys. Stat. Sol.* **7** (1964) 155.
83. J. CHIKAWA, *Japan. J. Appl. Phys.* **3** (1964) 229.
84. C. M. DRUM, *J. Appl. Phys.* **36** (1965) 816.
85. C. M. DRUM, *Phil Mag.* **11** (1965) 313.
86. C. M. DRUM and M. J. WHELAN, *Phil. Mag.* **11** (1965) 205.

Note Added During Proofing

Electron diffraction evidence supported by X-ray diffraction observations has been interpreted as showing the presence of both cubic and hexagonal phase materials in GaAs films [87]. X-ray Kossel line patterns have been used to measure lattice constants in order to study non-stoichiometry in GaAs. Point defects, present in concentrations up to about $10^{19}/cm^3$ after quenching, were identified as being primarily As vacancies, as a result of studies of the effects of annealing under high As vapour pressures [88]. A study of the variation of the degree of orientation in InAs films with As/In flux ratio changes using the three-temperature co-evaporation technique has also now been published [89].

87. T. PANKEY and J. E. DAVEY, *J. Appl. Phys.* **37** (1966) 1507.
88. H. R. POTTS and G. L. PEARSON, *ibid*, 2098.
89. J. E. JOHNSON, *ibid*, 2188.